CFSRC COLLOQUIUM

Proceedings of the Cold-Formed Steel Research Consortium Colloquium
20-22 October 2020 (cfsrc.org)

Mechanical properties of cold-formed thick-walled steels at elevated temperatures

Yuanqi Li[1], Zhen Nie[2]

Abstract

To study the mechanical properties of cold-formed thick-walled steels (with a thickness greater than 3mm) at elevated temperatures and the effect of cold-work forming on high-temperature performance of steels, this paper presents a series of specially designed material tests on Q345 steels. The coupons were pretreated by strengthening original plates to different strain levels and aging process. A total of 56 coupon tests were carried out using steady state test method for temperatures ranged from 20 to 600°C. Based on the tests, mechanical properties including yield strengths, ultimate strengths, elasticity modulus and stress-strain curves were obtained. Then, the influence of cold-work forming for steels at ambient and elevated temperatures were investigated by comparing failure modes, constitutive relationships and retention factors of steels with different strengthening degrees. Further, for predicting the mechanical properties of cold-formed thick-walled steels at elevated temperatures, a set of revision coefficients for hot-rolled steels was proposed depending on the tests data. Finally, verification tests on specimens cut from the typical cold-formed thick-walled steel tube have been conducted to validate the proposed prediction model.

1. Introduction

As the main components in light weight steel structural buildings, cold-formed steel (CFS) members are widely used around the world, approximately from 0.4 mm to 3.0mm thick, with grades from 200MPa to 1000Mpa [1]. Since the 1990s, along with the development of cold-forming technology and devices, cold-formed thick-walled steel sections with the thickness greater than 3mm are generalized in civil structures gradually [7]. Cold-formed thick-walled steel [6] sections with higher load bearing capacities, combined with advantages of cold-formed thin-walled steels (with the thickness under 3mm), make it possible that CFS can be extended from low-rise buildings to middle-rise and high-rise buildings. In this case, fire issues are essential for designing middle-rise and high-rise buildings using cold-formed thick-walled steel sections to meet higher fire safety requirements.

At ambient temperatures, the cold-formed effect is generally ignored for cold-formed thin-walled steel sections designing [1], although it can be calculated via equations [2-6]. For cold-formed thick-walled steel sections, the cold-formed effect should not be neglected, since more drastic mechanical processing and larger corner areas percentage bring greater influence of cold-formed effect on thick-walled sections. Moreover, aiming at material properties, some researchers have made their efforts on the yield strength prediction for steels of cold-formed thick-walled steel sections [7].

At elevated temperatures, the strain-hardening in cold-formed thick-walled steels is relieved with temperature rising, accordingly the mechanical properties of this type of steels may be different from hot-rolled steels and cold-formed thin-walled steels. Currently, the provision of high temperature material models for steels are based on hot-rolled steels [8-12]. The prediction model for mechanical properties of steels at elevated temperatures considering cold-formed effect has not been provided in existed codes. It is worth exploring how much of the impact there would be on high-temperature mechanical properties bringing from different degrees of strain-hardening. Based on this consideration, we deliberately transformed virgin hot-rolled steels into processed steels with three typical strengthening levels, and studied their mechanical properties at elevated temperatures along with original steels.

In this paper, taking the Q345 steel (nominal yield strength is 345MPa) with nominal thickness of 14mm as research objects, a special treatment of specimens and detailed high temperature coupon tests were conducted. Then, by comparing failure modes, constitutive relationships and reduction factors for different strengthening types of

[1] Professor, Ph.D., Department of Structural Engineering, Tongji University, Shanghai, China. Email: liyq@tongji.edu.cn
[2] Ph.D., Department of Structural Engineering, Tongji University, Shanghai, China. Email: 1310233@tongji.edu.cn

specimens, the impact of cold-formed effect on mechanical properties of steels at elevated temperatures is illustrated. Moreover, a prediction model of mechanical properties for the cold-formed thick-walled steels at elevated temperatures is proposed. Finally, coupon tests on the steels of the typical cold-formed thick-walled steel tube were finished to validate the proposed prediction model.

2. Experimental study

2.1 Pretreatment of test specimens

For low carbon steels, past investigations [7] on the influence of cold-formed effect indicate that the changes of mechanical properties due to cold-formed procedure at ambient temperatures are caused mainly by strain hardening and strain aging [1], as illustrated in Figure 1, in which curve A represents the stress-strain curve of the virgin material. Curve B is the unloading path after the elasticity region, curve C represents immediate reloading path, and curve D is the stress-strain curve of reloading after strain aging. It is obvious that the yield stresses of both curves C and D are higher than the yield stress of the virgin material and the ductility decreases after strain hardening and strain aging.

Based on this principle, it is convincing to assume that a steel plate is made up of numerous small fiber units, which follow stress-strain characteristics mentioned above in a single direction. In this way, although the strain hardening caused by cold-formed process is complex (including stretching, bending, squeezing etc.), by conducting a one-way elongation of original steels, a practical experimental method aiming on exploring the impact from cold-formed effect on temperature-dependent mechanical properties of steels was proposed in this research. Firstly, three discrete strengthening degrees, shown in Figure 2, are set: stretching the original steel (Q345, marked as Q0) to the yield plateau (marked as Q1), stretching the original steel to 5% overall strain (marked as Q2) and stretching the original steel to 10% overall strain (marked as Q3). Secondly, a typical dog-bone style cutting shape is designed to guarantee that the steel plate will be subject to uniaxial extension, as illustrated in Figure 3(a). Then, a tensile test machine with 1000kN capacity is used for elongating original plates, and an extensometer with 150mm gauge length is applied for acquiring stress-strain curves during overall stretching, as shown in Figure 3(b). Afterward, the aging effect was considered by storing stretched plates at ambient temperatures for one week. Additionally, in order to ensure that a 150mm even strengthening zone is created in the middle of the dog-bone shape plate, assisted finite element analysis was carried out before testing, of which the result is indicated in Figure 3(d). The colored part represents a zone with stress deference within 5% in Figure 3(d), proving that a uniform stress field core is able to be produced in central part of the dog-bone plate during extension. Finally, aiming at high temperature coupon tests, small bar-shaped specimens cut from pretreated plates (Q1~Q3) along strengthening direction and the original plate (marked as Q0) were experimental subjects in this study, as shown in Figure 4.

2.2 Test devices and procedure

Tests in this part were conducted in State Laboratory for Disaster Reduction in Civil Engineering-Fire Safety of Engineering Structures Testing Division in Tongji University. All coupons were cut by a wire cutting machine from pretreated steel plates mentioned above with diameter of 5.0mm. The dimension of the test specimens was determined by ISO standard [13], as presented in Figure 4(b). There were two screw threads at the end of specimens for fixing extension tension rods and two small lugs at the edge of parallel part for fixing extensometer system. The dimensions of specimens were average of that values measured at three points within gauge lengths by using a micrometer before testing.

The experiment setup is the EDC222 Doli testing system shown in Figure 5, which is an integrated closed loop digital control thermal and mechanical testing system. The tensile testing machine is an electronic servo system with 100kN capacity, which was calibrated before testing. A high temperature stove with a maximum temperature of 1200°C was employed in the testing. Three pairs of thermocouples binding separately on upper rod, surface of specimen and lower rod in a range of 150mm provided signals for accurate feedback control of specimen temperatures. In this way, a uniform temperature zone would be generated when the temperature of three thermal couples remained stable. The material for fixing thermocouples herein is the refractory heat insulation ceramic fiber cloth band. A set of linear displacement grating, including high temperature resistance extension rods, with a range of 12.5mm relative to 25mm gauge was used to acquire the deformation of specimens between the gauge lengths. Figure 6 gives details of the testing devices and Figure 7 presents the structure of high temperature extensometer system.

Tensile coupon tests were carried out by adopting the steady state test method. First, the specimen was heated up to a pre-selected temperature at a rate of 20°C/min. Free thermal expansion was allowed when heating up by keeping tensile load zero. The temperature levels selected in this experiment were 20°C, 100°C, 200°C, 300°C, 400°C, 500°C, and 600°C. The specimen was kept for 30~40min at this constant temperature until it reached the steady condition. Then the load was applied by controlling the displacement of the electronic tensile grip until failure while maintaining the set temperature degree. The displacement rate was set to 0.181mm/min, which was, specifically in elastic stage,

equivalent to a strain rate of 0.00007/s as the minimum rate specified by ISO standard [13]. Moreover, the sampling frequency was 10Hz. All the specimens were repeated twice for double checking.

3. Test results and discussion

3.1 Influence of cold-formed effect at ambient temperature

Before exploring the influence of cold-formed effect at elevated temperatures, it is essential to figure out the impact of cold-formed effect on mechanical properties of steels at ambient temperature. Table 1 gives average values of basic mechanical properties (elastic modulus, yield strength and ultimate strength) for steels with different strengthening types at ambient temperature. Also, the coefficient for the effect of cold-formed process (using η) is defined as multiples of the mechanical property value of the virgin steel, which represents the strengthening degree of steels.

For the elastic modulus, there is no significant change (less than 5%) between different strengthening types, which means it is reasonable to ignore the influence of cold-formed effect on elastic modulus of steels at ambient temperature. For the yield strength, it is 3%, 34% and 65% higher for Q1, Q2 and Q3 separately than that of the virgin steel. However, for the ultimate strength, very limited raising (less than 10%) for strengthened steels (Q1, Q2 and Q3) was illustrated at these tests.

In order to verify the rationality of the strengthening method adopted in this research, constitutive relationships for different strengthening types at ambient temperature are put together (shown in Figure 8) and compared with the ideal stress-strain characteristics of strain hardened and strain aged steel (shown in Figure 1). Since two curves in each condition (from repeated experiments) come quite close, as depicted in Figure 8, one of the curves in each case is picked out to making further comparison clearly. Then, focusing on ascending branch of curves, as shown in Figure 9(a), stress-strain curves of steels with different strengthening types present quit different shapes: elastic stages of strengthened steels (Q1, Q2, and Q3) fit closely with the original steel (Q0); curves of strengthened steels lose yield platform apparently; and knee points of curves move up from Q0 to Q3. Moreover, based on strengthening paths depicted in Figure 2, for better observing the influence of strain hardening and aging, these curves were shifted to right with 0.5%, 5% and 10% strain, shown in Figure 7(b). Real stress-strain relationships considering strain hardening and aging (shifted curves shown in Figure 7(c)) are consistent with ideal characteristics curves in Figure 1, indicating that the strengthened curve can be regarded as a reloading curve starting from the unloading position (virgin steel) with higher yield and ultimate strength. Thus, the proposed steel strengthening method accord with hardening and aging principle of steels, and strengthened steels are appropriate to be used as research targets in high-temperature test study.

3.2 Failure modes

Figure 10 presents the failure modes of tested coupons with different strengthening degrees. The vernier caliper, as a measuring scale for reference, read 25mm in the picture. All specimens fractured within the gauge length scope expectedly, which means the stress-strain curves recorded from data acquisition system were real stress-strain relationships within the gauge length. For all tested cases, visually noticeable elongation and necking of the coupons were occurred at ambient and elevated temperatures. A similar trend is seen in the elongation development along with temperature rising for steels with different strengthening degrees. It is interesting to find that steels lost their ductility obviously when the temperature increased from 20°C to 200°C. This material behavior may be attributed to chemical transformations taking place in the steel base. After 300°C, since chemical reactions were taken over by temperature effects as the dominate factor, the elongation of specimens grew continually as expected. Up to 600°C, the ductility of specimens was significantly higher than that of lower temperatures.

3.3 Constitutive relationship

Since the measurement range of the displacement grating is 12.5mm, the stress-strain curves are given within the total strain of 0.5. Stress-strain curves of Q0 (Virgin steels) at different temperatures are shown in Figure 11, which are the foundation of comparative discussion in this section.

In order to explore the effect of cold-formed process on mechanical properties of steels at elevated temperatures directly, stress-strain complete curves and up-leg curves of steels with different strengthening types (Q0~Q3) are put together in one diagram at each temperature point from 100°C to 600°C, as shown in Figure 12~Figure 17. Below 500°C, knee points ascend gradually along with strengthening degrees rising at the same temperature condition, but peak points have little difference. Shape difference of stress-strain curves of steels with different strengthening types narrow down with increasing temperatures. After 500°C, curves of Q0~Q3 steels tend to be accordant. In the meantime, elastic segment of those curves at the same temperature are basically coincided with each other.

Furthermore, constitutive curves with different strengthening types at 400°C~600°C are presented together in Figure 18. Obviously, the stress-strain curves of Q0~Q3 steels pinch into a small zone and nearly overlap with each other when temperatures reach 600°C. It is indicated by this

phenomenon that the influence of cold-formed effect on mechanical properties of steels was eliminated generally over 600°C. Based on the knowledge of heat treatment for steel [14], the critical temperature Ac1 (pearlite transforms into austenite at this temperature point) is over 600ºC for low carbon steel, and the critical temperature Ac3 (eutectoid point) is above 700ºC for low carbon steel. Strengthened steels experience partial or full annealing when heated over these critical temperatures, and their ductility and strength recovery partially or fully to the original level. Hence, there are two major factors on determining mechanical properties of strengthened steels at elevated temperatures: 1) the deterioration of mechanical properties; 2) the reduction of cold-formed effect. Based on this general conclusion, more specific parametric analysis is needed in later discussion to quantitatively study mechanical properties of steels considering cold-formed effect at elevated temperatures.

3.4 Retention factors

Primarily, Table 1 gives the tensile test results of Q0~Q3 steels at ambient temperature, which are fundamental parameters for calculating their high temperature material properties. Retention factors for the elastic modulus and yield strength were computed as the ratios of material properties at high temperatures to their values at ambient conditions. Results are shown in Table 2. The elastic modulus was calculated by fitting the initial portion of the stress-strain curves via using the least squares method, following ISO standard [13]. For the curves with smooth and long yield plataeu, the yield strength was taken as the average value of stresses in the plataeu. Then for the gradual yielding cases, the yield strength was determined by the 0.2% proof stress method, which uses the intersection point of the stress-strain curve and the proportional line offset by 0.2% strain. Therefore, by separating the influence of temperatures on the deterioration of mechanical properties apart, normalized mechanical properties of steels with different strengthening degrees at the same temperature condition are able to be compared to explore reduction rules of cold-formed effect at elevated temperatures.

Figure 19 and Figure 20 provide the retention factors for Q0~Q3 steels obtained through coupon tests from this study and current design codes [8-12]. For elastic modulus, as shown in Figure 19, there is no obvious difference between strengthened steels (Q1~Q3) on reduction trend at elevated temperatures. Generally, strengthened steels drop slower than the original steel (Q0) before 400°C, however degradation rate of strengthened steels become faster over 400°C. For yield strength, as shown in Figure 20, strengthened steels descend slowly first and fast afterwards compared with the original steel, which is similar with the elastic modulus reduction trend. Specifically, after 400°C, the rate of decline accelerates with the strengthening degree rising (from Q1 to Q3).

By comparing tests data with current design codes [8-12], retention factors from existing steel design codes are generally unsafe, especially for yield strength prediction. In addition, the prediction curves of standards are fitted from large number of tests data generally, and using one-time experiment data to directly propose new prediction curves of retention factors for strengthened steels is hardly representative. Therefore, for strengthened steels, it is reasonable to figure out the relationships on mechanical properties between strengthened steels and the original steel, then to propose modification factors depending on the strengthening degrees for revising the prediction models provided in current codes which are based on hot-rolled steels.

4. Prediction model

4.1 Calculation path

Generally, in fire design, the calculation method of mechanical properties for steels at elevated temperatures is as follow:

$$a_T = a_{20} \times A_T \tag{1}$$

where a_{20} and a_T are one of mechanical properties (e.g. elastic modulus, yield strength etc.) for steels at ambient and elevated temperatures, and A_T is the retention factor of this mechanical property at *T*(°C) which can be acquired from related standards.

In order to thoroughly separate two impacts on determining mechanical properties of strengthened steels at elevated temperatures, the equation (1) is transformed as:

$$\begin{aligned} a_{n,T} = a_{n,20} \times A_{n,T} &= \left(a_{n,20}\frac{a_{n,20}}{a_{0,20}}\right) \times \left(A_{0,T}\frac{A_{n,T}}{A_{0,T}}\right) \\ &= \eta_{n,20} \times \beta_{n,T} \times a_{0,20} \times A_{0,T} \end{aligned} \tag{2}$$

where $\eta_{n,20} = a_{n,20}/a_{0,20}$ is the coefficient of cold-formed effect at ambient temperature (e.g. η_E and η_f). $\beta_{n,T} = A_{n,T}/A_{0,T}$ is a new temperature related factor. $a_{0,20} \times A_{0,T}$ is the mechanical properties of the original steel (hot-rolled steels) at elevated temperatures, which is usually provided by steel structure design codes.

It is clear that $\eta_{n,T} = \eta_{n,20} \times \beta_{n,T}$ based on the equation (2), and then $\beta_{n,T} = \eta_{n,T}/\eta_{n,20}$. In fact, $\beta_{n,T}$ is the reduction factor for the coefficient of cold-formed effect at elevated temperatures. In this case, two major factors on mechanical properties of strengthened steels at elevated temperatures are completely separated: the deterioration of mechanical

properties (i.e. $A_{0,T}$ is the retention factor for $a_{0,20}$) and the reduction of cold-formed effect (i.e. $\beta_{n,T}$ is the reduction factor for $\eta_{n,20}$). Furthermore, it is possible to propose equations for calculating mechanical properties of strengthened steels by adding modification factors in front of mechanical properties of the original steel (hot-rolled steel) at elevated temperatures.

The temperature factor for the coefficient of cold-formed effect for elastic modulus ($\beta_{E,T}$) and yield strength ($\beta_{f,T}$) at elevated temperatures are listed in Table 3 and Table 4. Also, temperature-dependent curves of these factors are presented in Figure 21 and Figure 22. For elastic modulus, $\beta_{E,T}$ follows the very similar trend with $\eta_{E,T}$ when temperatures rising, as the influence of cold-formed effect on elastic modulus of steels at ambient temperature is almost negligible. For yield strength, curves of $\beta_{f,T}$ agree with each other essentially before 400°C. The descent rate of $\beta_{f,T}$ positively correlates with the strengthening degree (based on the η_f at ambient temperature) after 400°C.

4.2 Prediction for elastic modulus

Due to the weak dependence of the strengthening degree of steels on $\beta_{E,T}$, a single equation with one variable (the temperature) provided here for calculating the temperature factor for the coefficient of cold-formed effect for elastic modulus by fitting (polynomial fitting) the scatters of all strengthened steels. Figure 23 is the fitting curve of $\beta_{E,T}$ for strengthened steels along with tested data scatters. Based on the equation (2), the elastic modulus of strengthened steels at elevated temperatures is as follow:

$$E_T = \eta_E \times \beta_{E,T} \times E_{0,T} \quad (3)$$

$$\beta_{E,T} = 1 \qquad 20℃ \le T \le 200℃$$

$$\beta_{E,T} = 6.817 \times 10^{-9} \times T^3 - 1.147 \times 10^{-5} \times T^2 + 5.35 \times 10^{-3} \times T + 3.339 \times 10^{-1} \qquad 200℃ \le T \le 600℃$$

where $\eta_E = 1$, and $E_{0,T}$ is the elastic modulus for the original steel (hot-rolled steel) at elevated temperatures which can be taken from current codes [8-12] during fire design calculations.

4.3 Prediction for yield strength

Before 400°C, a single equation with one variable (the temperature) was fitted (polynomial fitting) for calculating the temperature factor for the coefficient of cold-formed effect for yield strength, as Equation (4). Considering $\beta_{f,T}$ is related to both the temperature and strengthening degree (based on the η_f at ambient temperature) after 400°C. Two times of linear fitting were conducted: 1) fitting of $\beta_{f,T}$ for steels with different strengthening degree, as equation (5), of which parameters are listed in Table 5; 2) fitting of constant terms and linear terms for $\beta_{f,T}$, as equation (6), of which results are listed in Table 6. Figure 24 is the final fitting results of for strengthened steels, which is a 3-D surface in T-η_f-$\beta_{f,T}$ coordinates.

$$\beta_{f,T} = 3.003 \times 10^{-11} \times T^4 - 3.731 \times 10^{-8} \times T^3 + 1.19 \times 10^{-5} \times T^2 - 2.676 \times 10^{-4} \times T + 1 \qquad 20℃ \le T \le 400℃ \quad (4)$$

$$\beta_{f,T} = A_0 + A_1 \times T \qquad 400℃ \le T \le 600℃ \quad (5)$$

$$A_i = a_0 + a_1 \times \eta_f \ (i=0,1) \quad (6)$$

Based on the equation (2), the yield strength of strengthened steels at elevated temperatures is as follow:

$$f_T = \eta_f \times \beta_{f,T} \times f_{0,T} \quad (7)$$

$$\beta_{f,T} = 3.003 \times 10^{-11} \times T^4 - 3.731 \times 10^{-8} \times T^3 + 1.19 \times 10^{-5} \times T^2 - 2.676 \times 10^{-4} \times T + 1 \qquad 20℃ \le T \le 400℃$$

$$\beta_{f,T} = 1.324\eta_f + \left(2.944 \times 10^{-3} - 3.31 \times 10^{-3}\eta_f\right) \times T \qquad 400℃ \le T \le 600℃$$

where η_f for different parts of the cold-formed thick-walled steel member section can be calculated using standards equations [2-6], and $f_{0,T}$ is the yield strength for the original steel (hot-rolled steel) at elevated temperatures which can be taken from current codes [8-12] during fire design calculations.

4.4 Comparison between predicted and tested results

In order to verify the rationality of the fitting process in proposing the prediction equations, comparison between predicted and tested results are shown in Table 7 and Table 8. Obviously, all mean values of test-prediction ratio are close to 1, and corresponding coefficients of variation are less than 10%. In conclusion, proposed equations can provide a precise and simple prediction for mechanical properties of steels considering the cold-formed effect at elevated temperatures.

5. Verification Test

5.1 Test specimens

Dimension parameters of selected typical cold-formed thick-wall steel tube are listed in Table 7. Since mechanical properties of the cold-formed steel section considering cold-formed effect were determined by flat part, corner part and weld seam [7]. Specimens cut from flat, corner and weld parts were tested, as shown in Figure 25(a). Also, specimens extracted from the same batch base metal (hot-rolled steel plate) which was used for processing this steel tube were tested as the reference group. All coupons were cut by a wire cutting machine from both the base metal and

the cold-formed thick-wall steel tube. Dimensions of the test specimens were determined by ISO standard [13], as presented in Figure 25(b) and (c). For corner part specimens, both ends were flattened for clamping easily and avoiding eccentric load when testing.

5.2 Test devices and procedure

Tests in this section were conducted in fire safety laboratory in the China University of Mining and Technology. The experiment setup is the MTS Landmark testing system shown in Figure 26. The tensile testing machine is the MTS hydraulic servo system with 200kN capacity. The heating device was the MTS 653 high-temperature furnace with a maximum temperature of 1400°C. A high-temperature extensometer with a 25mm gauge length was adopted to measure the strains of the steel specimens during test. Three thermocouples were bundled on the upper, middle, and lower parts of the specimens to sample real time temperatures.

As the cross-section areas of corner specimens were hard to be measured directly, six 10mm-high pieces located within the gauge length were cut from two different backup specimens. Then, the weight of each piece could be measured using electronic balance, and the area could be calculated through dividing the mass by the density and the height. In previous study [7], the small piece was cut from the tested coupons due to the minor change of the section area of the parallel part (besides fracture and necking part) in ambient-temperature coupon tests. However, the cross-section areas of specimens significantly reduced after high-temperatures tensile tests as shown in Figure 27. Thus, the mean value of areas of six small pieces mentioned above was adopted as the unified area for all corner part specimens when calculating mechanical properties.

The tests were carried out by adopting the steady state test method. First, the specimen was heated up to a pre-selected temperature at a rate of 20°C/min. Free thermal expansion was allowed when heating up by keeping tensile load zero. The temperature levels selected in the validation test were 20°C, 300°C, 400°C, 500°C, and 600°C. The specimen was kept for 30min at the target temperature until it reached the steady condition. Then the load was applied by controlling the displacement of the lower grip until failure while maintaining the preset temperature degree. The displacement rate was set to 0.3mm/min. One-time test for each temperature condition was conducted unless the test failed.

5.3 Test results and discussion

In this part, the results of the test are discussed briefly to reveal the mechanical properties of cold-formed thick-walled steels at elevated temperatures.

Figure 27 present failure modes for different tested specimens. For base metal, flat part and corner part specimens, significant increase on the elongation of tested coupons is observed at 600°C, indicating that steels were fully or partially annealed in the furnace at 600°C and lost all or part of the cold-formed effect developed in rolling and bending process. For weld seam specimens, the ductility at different temperatures seems unstable, perhaps due to the randomness of defects in weld seams.

Meanwhile, stress-strain curves of all tested specimens are shown in Figure 28. Stress-strain curves of base metal specimens are typical hot-roll steels constitutive relationships as depicted in Figure 32(a). The yield plateaus with multiple yield points are the result of interrupted motion of the Luders band along the specimen. The movement of dislocations near the band front becomes locked when temperature reaches 300°C, and thus yield plateaus are disappeared over this temperature [15]. Curves of flat part, corner part and weld seam specimens are of the gradual yielding type and similar with curves of Q1~Q3 in previous tests. Specifically, at ambient temperature, curves of flat part specimens are similar with Q1 steels of which yield ratio is relatively low; curves of corner part and weld seam specimens are similar with Q3 steels of which yield ratio is much higher. With temperatures rising, shapes and peak point of curves of different part specimens gradually approach with each other, which is very consistent the phenomenon presented in Figure 18.

Table 8 gives mechanical properties of cold-formed thick-walled steels at ambient temperature as the base for calculation mechanical properties at elevated temperatures. Here, η_E of steels from different parts of the section are close to 1, proofing that the influence of cold-formed effect on the elastic modulus can be dismissed at ambient temperature. For flat part, corner part and weld seam steels, η_f was 1.23, 1.69 and 1.62 separately. Also, raising of the ultimate strength for steels cut from the cold-formed thick-walled steel section is relatively lower than that of the yield strength. At the same time, retention factors for the elastic modulus and yield strength of all tested specimens in this verification test are listed in Table 9.

5.4 Validation of proposed prediction model

Last and the most important, after acquiring mechanical properties of base metal, flat part, corner part and weld seam steels from the real cold-formed thick-walled steel tube at elevated temperatures, it is reasonable to validate the applicability of the proposed prediction model. Based on the equation (4) and (8), to take mechanical properties of base metal specimens as known variables, comparisons between tested and predicted results for both the elastic modulus and yield strength are arranged in Table 10 and

Table 9. Additionally, for the elastic modulus, η_E was 1; and for the yield strength, η_f was taken from Table 8. It is clear that predicted values are quite close to tested results for all specimens, strongly indicating that the prediction model proposed in this study is capable to calculate mechanical properties of cold-formed thick-walled steels at elevated temperatures.

6. Conclusions

In this study, a series of coupon tests on steels with different strengthening degrees (based on the coefficient of cold-formed effect at ambient temperature) and a set of verification test on steels from a real cold-formed thick-walled steel tube were conducted. The influence of cold-formed effect on mechanical properties of steels at elevated temperatures was explored, and the prediction model of mechanical properties of steels considering cold-formed effect was put forward. The main conclusions are as follows:

1) At ambient temperature, the cold-formed effect can significantly improve the yield strength and ultimate strength of steels, but has little effect on the elastic modulus.

2) Before 400°C, the constitutive curves of steels with different strengthening degrees are obviously different from each other at the same temperature condition. With the increase of temperature, the difference decreases gradually, and the constitutive curves of steels with different strengthening degrees basically coincide at 600°C.

3) At high temperatures, the influence of cold-formed effect on the elastic modulus of steel is still limited, while the effect on yield strength is gradually eliminated with the increase of temperatures.

4) The degradation modes on mechanical properties of the strengthened steels and the original steels are quite different at elevated temperatures. Specifically, the degradation rate of yield strength has a strong positive correlation with the strengthening degree after 400°C.

5) Two major factors on mechanical properties of strengthened steels at elevated temperatures were completely separated: the deterioration of mechanical properties and the reduction of cold-formed effect. Then, by adding modification factors in front of mechanical properties of the original steel (hot-rolled steel) at elevated temperatures, equations for calculating mechanical properties of strengthened steels were proposed.

6) The proposed prediction model was well verified for predicting mechanical properties of different parts of cold-formed thick-walled steel member sections at elevated temperatures.

7. Acknowledgments

The authors are grateful to the financial support of the National Natural Science Foundation of China (No. 51478332 and No. 51538002).

References

[1] W. W. Yu, Cold-formed steel design, Wiley, New York, 2010.
[2] AISI S100. North American specification for the design of cold-formed steel structural members. American Iron and Steel Institute, 2016.
[3] AS/NZS 4600: Australian/New Zealand standard cold-formed steel structures. 2018.
[4] BS 5950-5: Structural use of steelwork in building-part 5: code of practice for design of cold-formed sections. British Standards Institution, 1998.
[5] EN 1993-1-3 Eurocode 3: design of steel structures: part 1-3: general rules: supplementary rules for cold-formed members and sheeting. Brussels: European Committee for Standardization, 2006.
[6] GB 50018. Technical code of cold-formed steel structures (in Chinese). Beijing, China, 2016.
[7] Gongwen Li, Yuanqi Li, Overall stability behavior of axially compressed cold-formed thick-walled steel tubes. Thin-Walled Structures, 2018, 125: 234-244.
[8] AISC 360-05. Specification for structural steel buildings. American Institute of Steel Construction, 2005.
[9] AS/NZS 4100: Steel structures. Sydney: Standards Australia, 1998.
[10] BS 5950-8: 1990. Structural use of steelwork in building-part 8: code of practice for fire resistant design. British Standards Institution, 1998.
[11] CECS 200. Technical code for fire safety of steel structure in buildings (in Chinese). Beijing, China, 2016.
[12] EN 1993-1-2 Eurocode 3: design of steel structures: part 1-2: general rules: structural fire design. Brussels: European Committee for Standardization, 2005.
[13] International Standard. ISO 6892-2: Metallic materials-tensile testing-part 2: method of test at elevated temperature. Switzerland, 2011.
[14] Krauss, G., Principles of heat treatment of steel. Ohio: American Society for Metals. Metals Park, 1980.
[15] E.O. Hall, Yield point phenomena in metals and alloys, Plenum Press, New York, 1970.

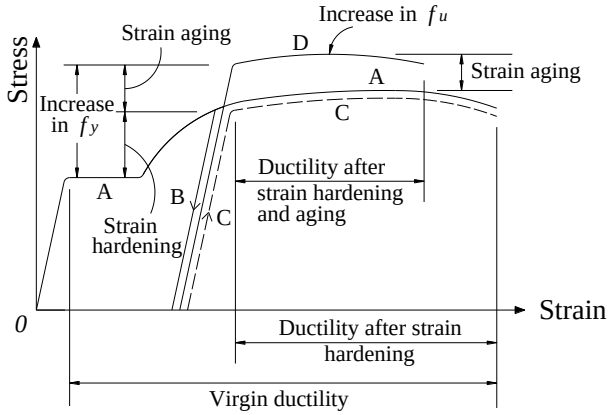

Figure 1: Effects of strain hardening and strain aging on stress-strain characteristics

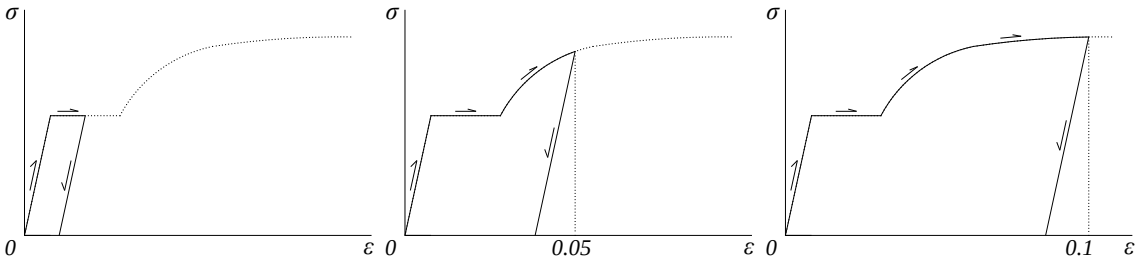

(a) Q1 (b) Q2 (c) Q3

Figure 2: strengthening paths

(a) Original plates (b) Overall stretching (c) Aging process

Figure 3: Strengthening process Different

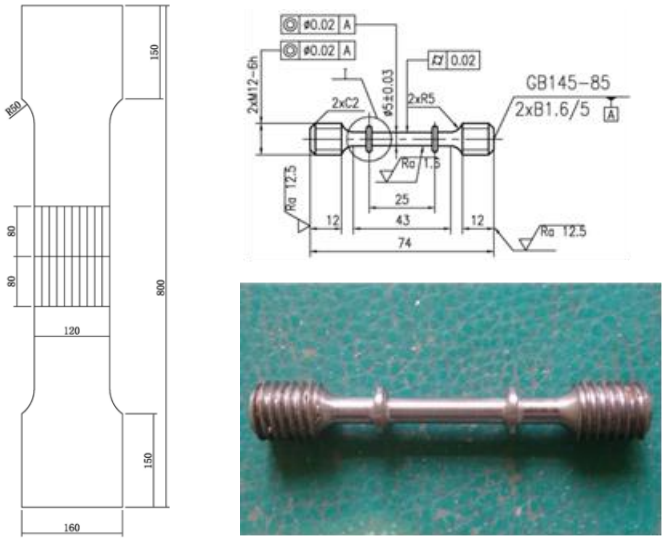

(a) Cutting lofting (b) Dimensions of specimens

Figure 4: Specimens for high temperature coupon tests

Figure 5: Testing system

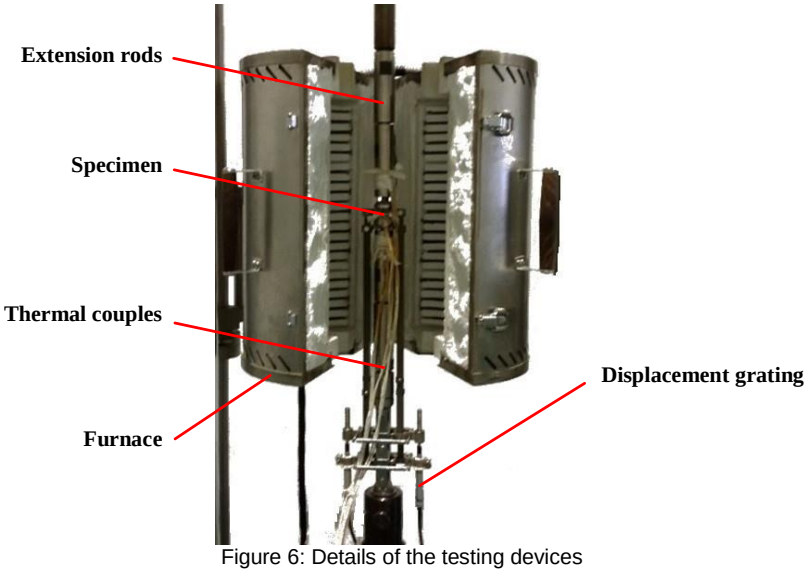

Figure 6: Details of the testing devices

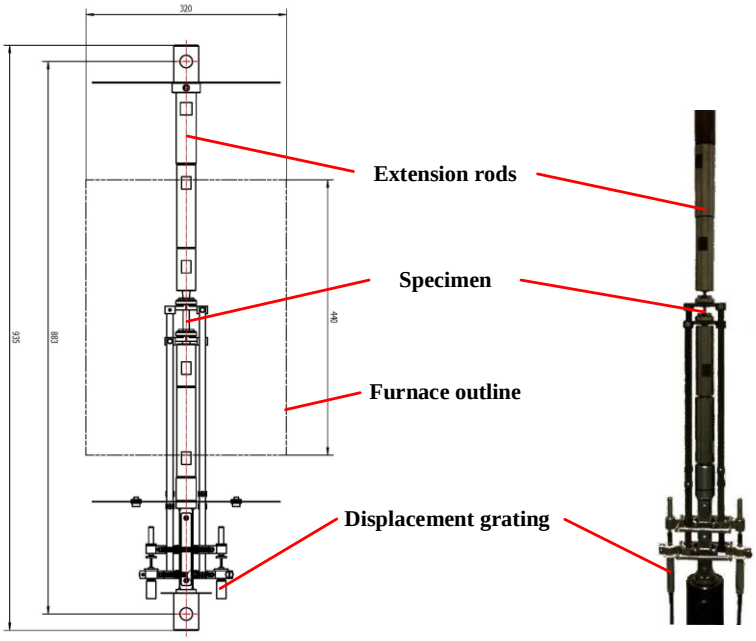

Figure 7: High temperature extensometer system

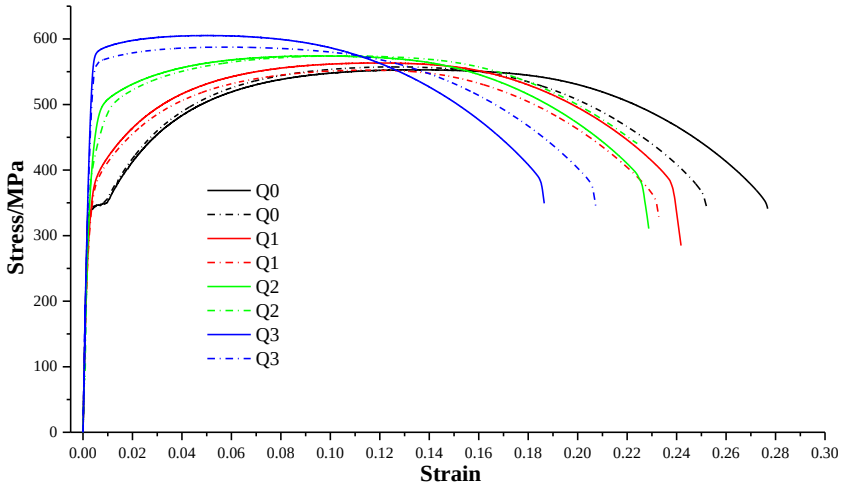

Figure 8: Comparison on constitutive relationship between different strengthening types at ambient temperature

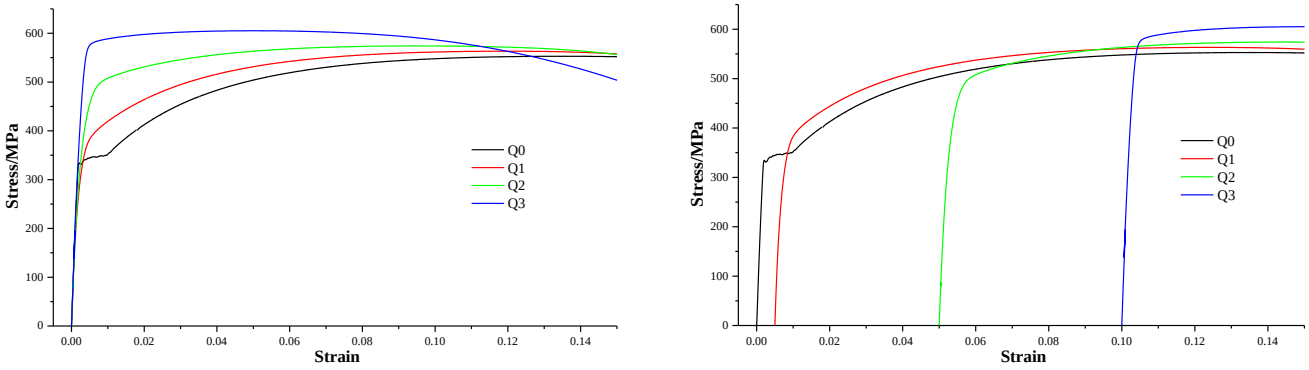

(a) Ascending branch of curves

(b) Shifted curves

Figure 9: Validation of strengthening paths

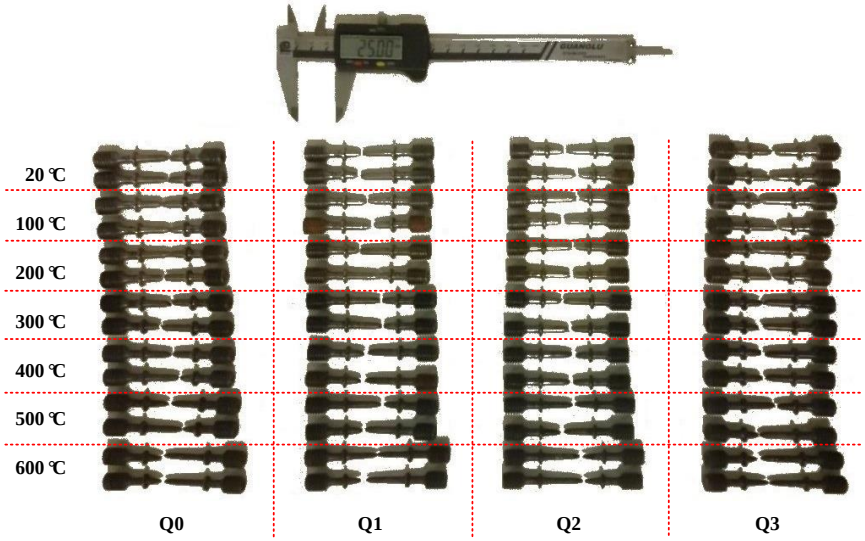

Figure 10: Failure modes for tested specimens

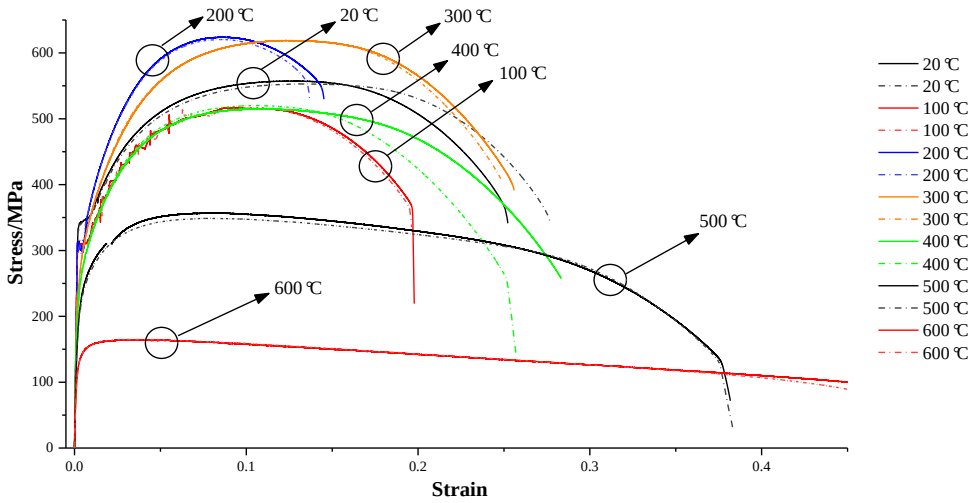

Figure 11: Stress-strain curves of Q0 (Virgin steels) at different temperatures

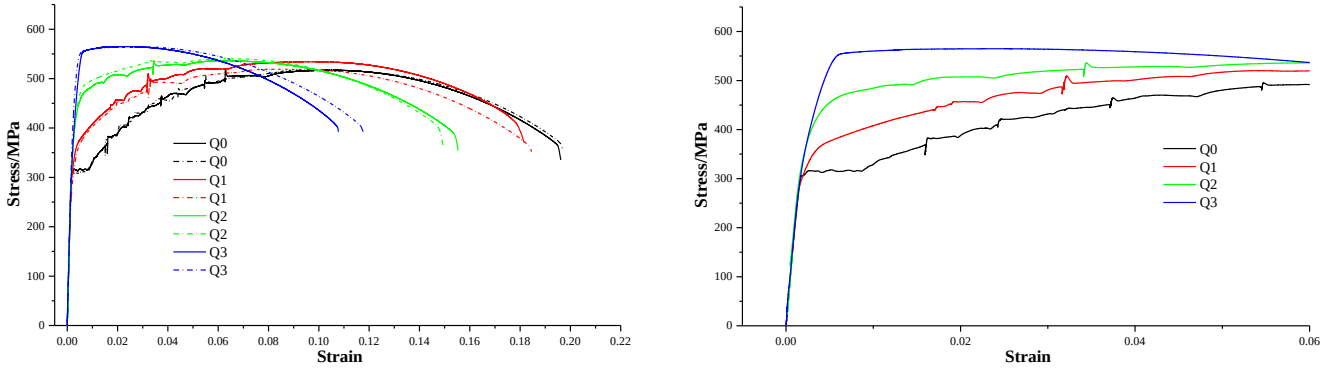

(a) Complete curves (b) Up-leg curves

Figure 12: Comparison on constitutive relationships between different strengthening types at 100ºC

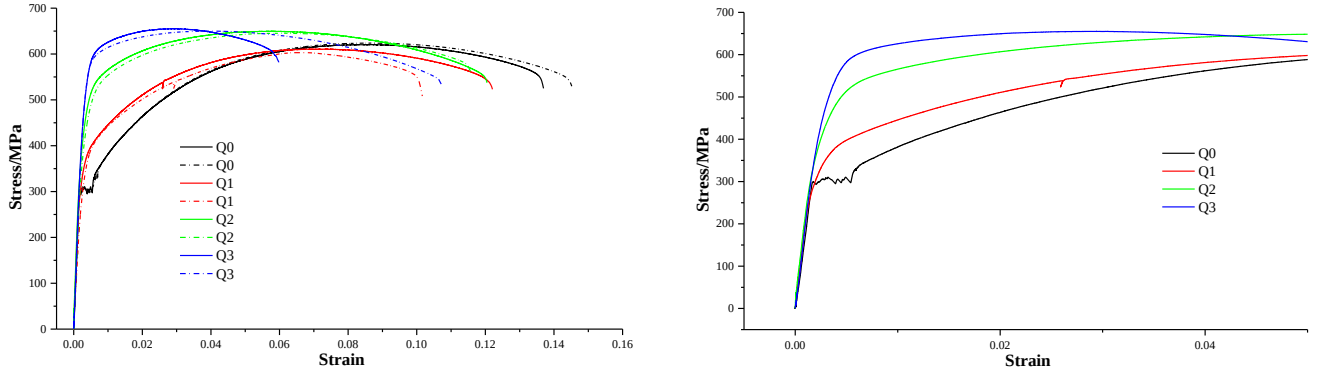

(a) Complete curves (b) Up-leg curves

Figure 13: Comparison on constitutive relationships between different strengthening types at 200ºC

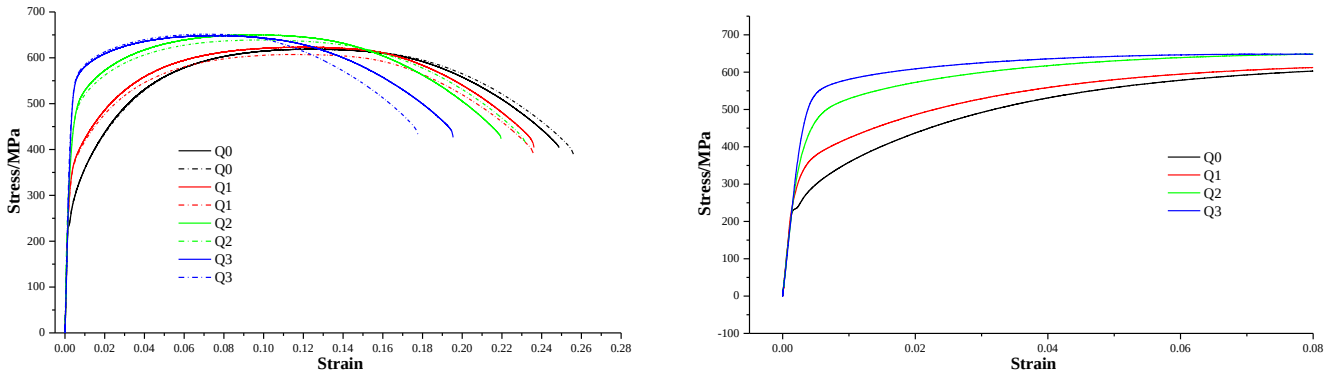

(a) Complete curves (b) Up-leg curves

Figure 14: Comparison on constitutive relationships between different strengthening types at 300ºC

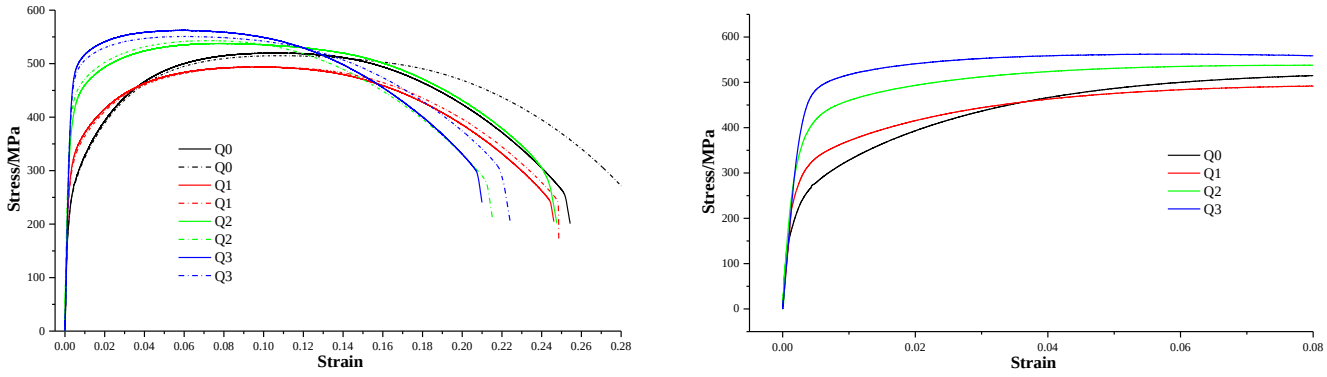

(a) Complete curves (b) Up-leg curves

Figure 15: Comparison on constitutive relationships between different strengthening types at 400ºC

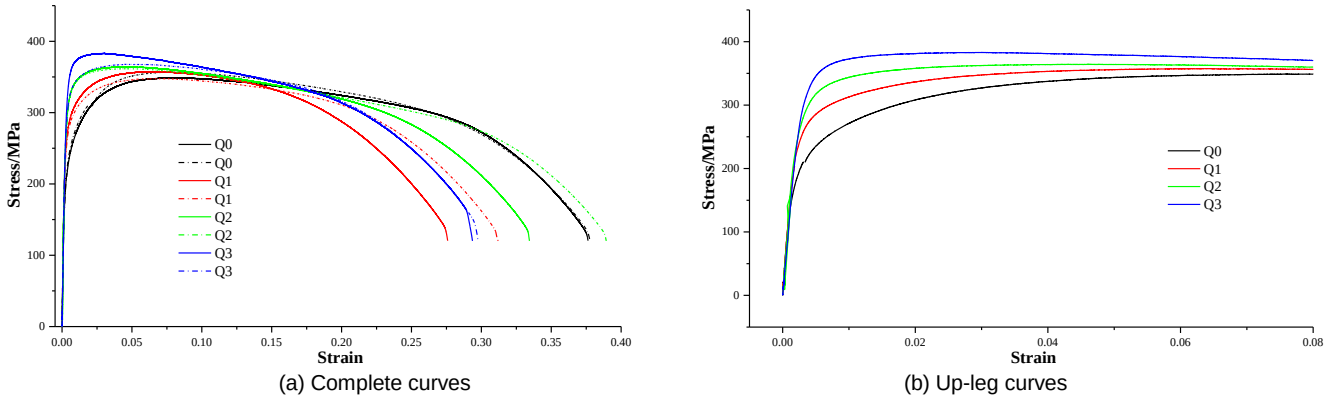

(a) Complete curves (b) Up-leg curves

Figure 16: Comparison on constitutive relationships between different strengthening types at 500ºC

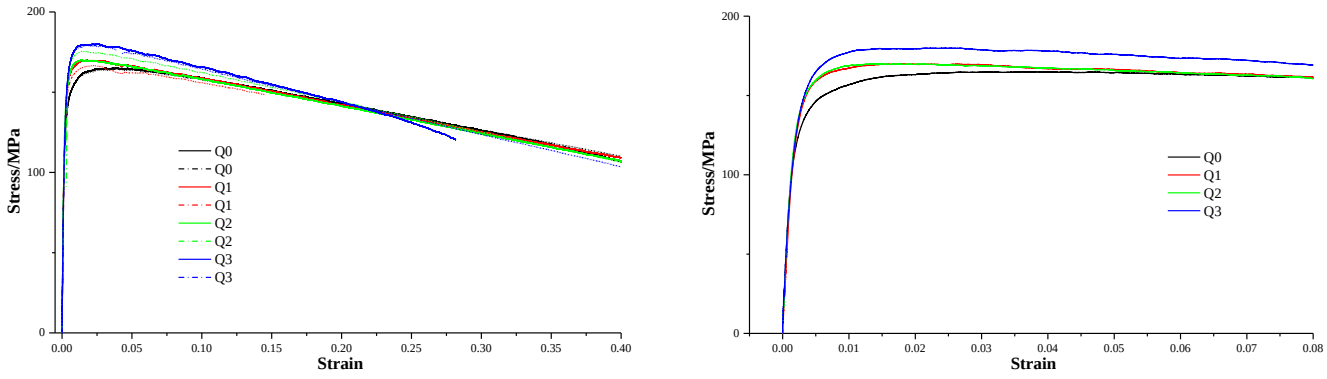

(a) Complete curves (b) Up-leg curves

Figure 17: Comparison on constitutive relationships between different strengthening types at 600ºC

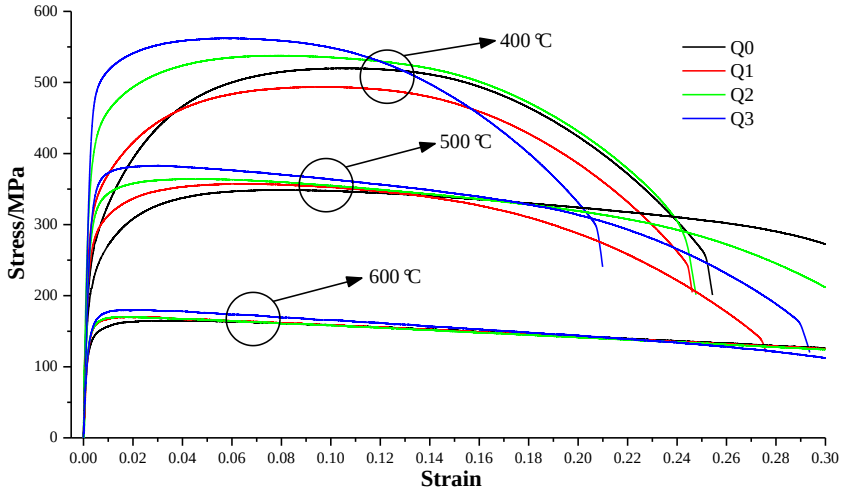

Figure 18: Constitutive relationships with different strengthening types at 400ºC, 500ºC and 600ºC

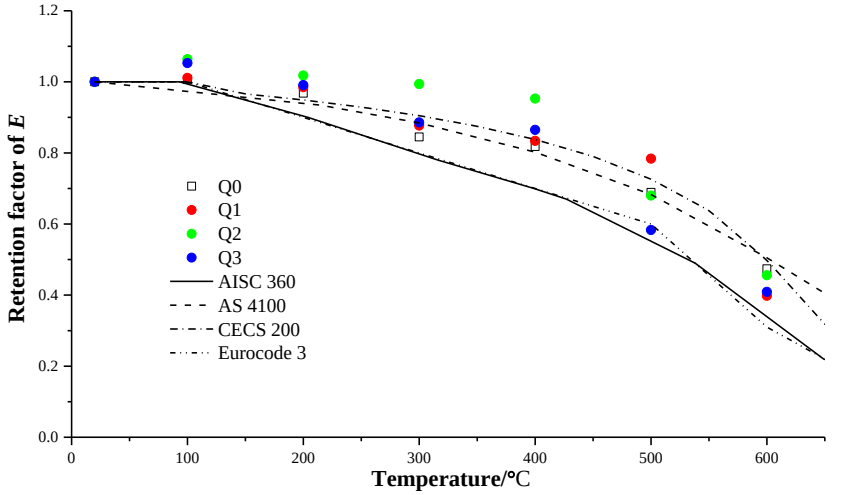

Figure 19: Comparison between standards and tested results for retention factors of elastic modulus

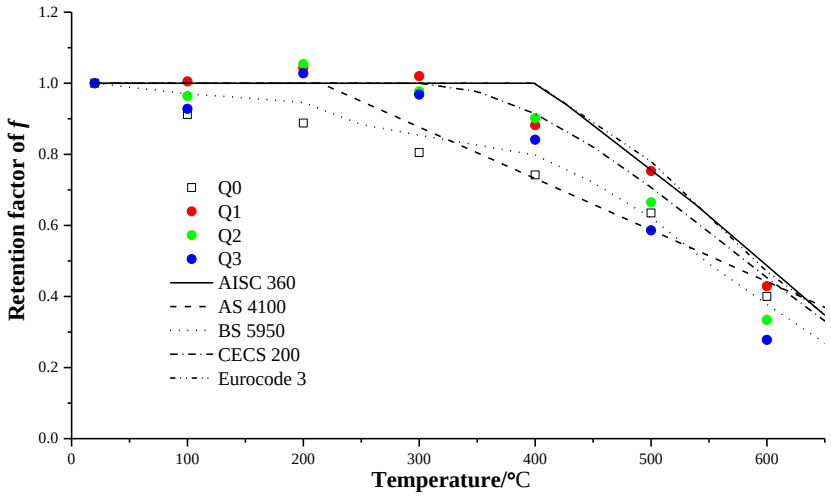

Figure 20: Comparison between standards and tested results for retention factors of yield strength

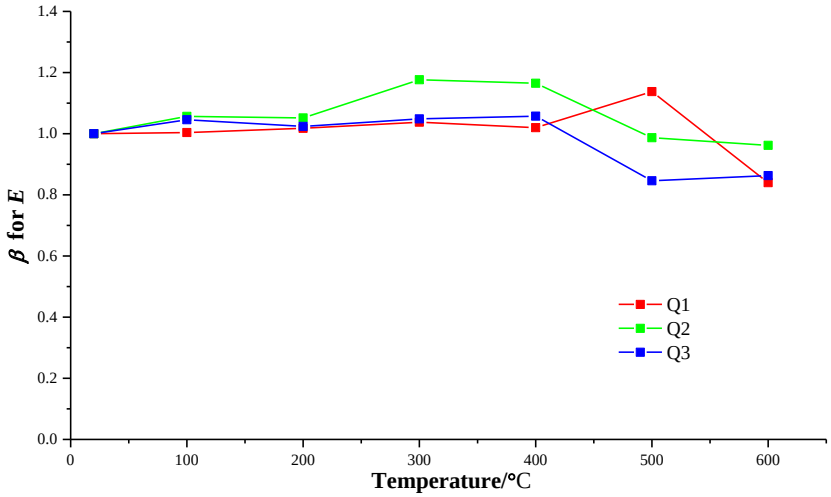

Figure 21: The temperature factor for the coefficient of cold-formed effect for elastic modulus

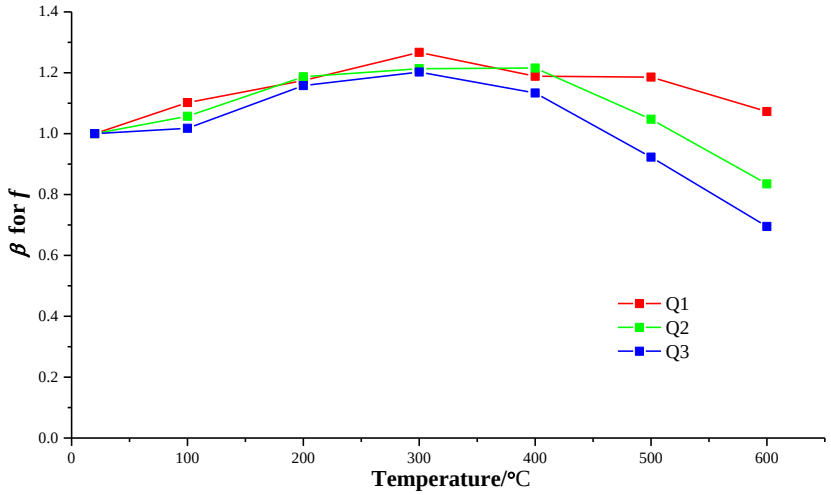

Figure 22: The temperature factor for the coefficient of cold-formed effect for yield strength

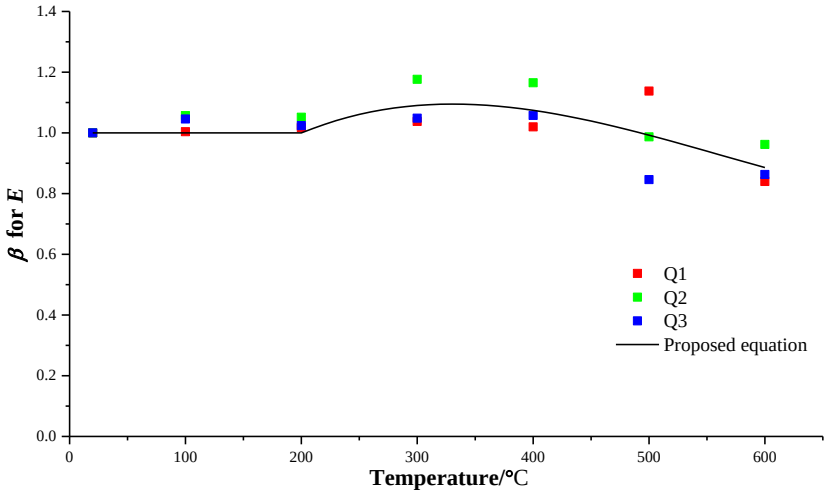

Figure 23: Fitting for the temperature factor $\beta_{E,T}$

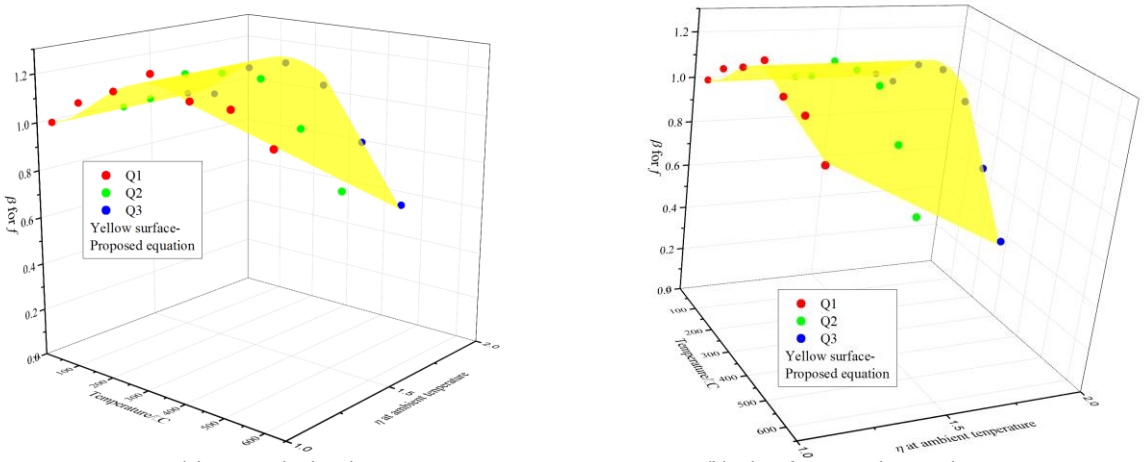

(a) Isometric drawing

(b) View from another angle

Figure 24: Fitting for the temperature factor $\beta_{f,T}$

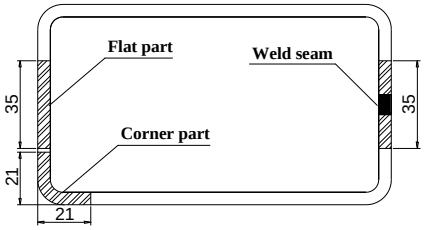

(a) Definition of specimens

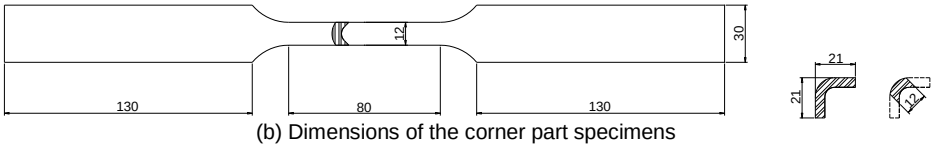

(b) Dimensions of the corner part specimens

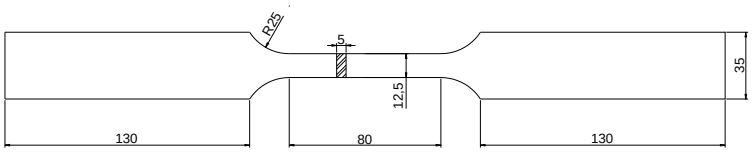

(c) Dimensions of flat specimens (base metal, flat part and weld seam)

Figure 25: Specimens of the verification test

(a) Test setup for ambient temperature

(b) Test setup for high temperatures

Figure 26: Test equipment of the verification test

(a) Base metal

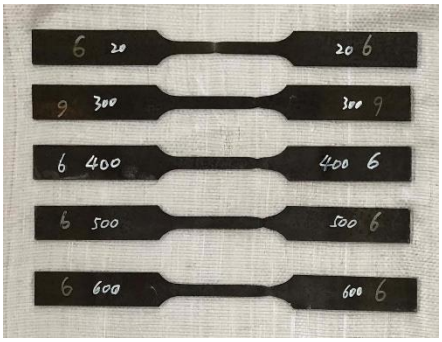

(b) Flat part

(c) Corner part

(d) Weld seam

Figure 27: Failure modes for tested specimens

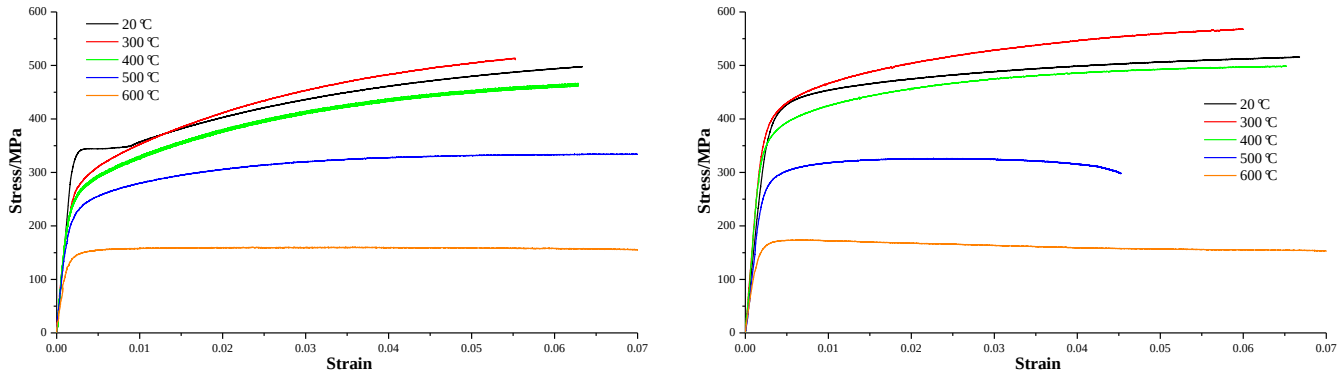

(a) Base metal

(b) Flat part

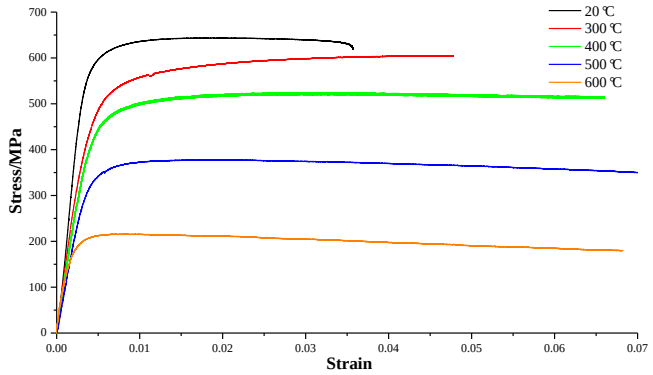

(c) Corner part

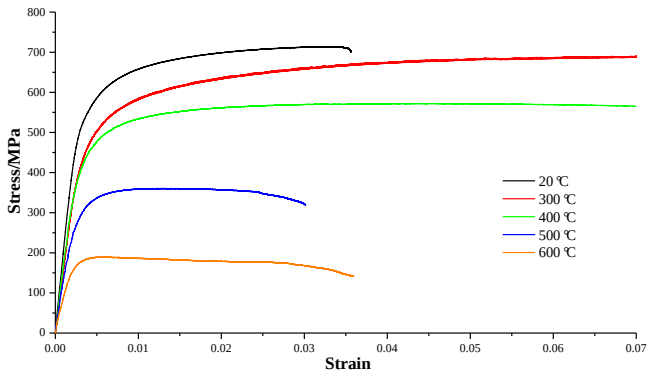

(d) Weld seam

Figure 28: Constitutive relationships of different specimens in the verification test

Table 1: Influence of cold-formed effect on mechanical properties of steels at ambient temperature

Strengthening type	Q0 (Virgin steel)	Q1	Q2	Q3
Elastic modulus *E* (GPa)	202.7	200.7	196.1	199.2
The coefficient of cold-formed effect for elastic modulus $\eta_E = E/E(\mathrm{Q0})$	1.00	0.99	0.97	0.98
Yield strength *f* (MPa)	341.9	353.4	459.1	563.6
The coefficient of cold-formed effect for yield strength $\eta_f = f/f(\mathrm{Q0})$	1.00	1.03	1.34	1.65
Ultimate strength f_u (MPa)	555.2	557.9	569.8	596.4
The coefficient of cold-formed effect for ultimate strength $\eta_{f_u} = f_u/f_u(\mathrm{Q0})$	1.00	1.01	1.03	1.07

Table 2: Retention factors for the elastic modulus and yield strength

T(°C)	Q0		Q1		Q2		Q3	
	E_T/E_{20}	f_T/f_{20}	E_T/E_{20}	f_T/f_{20}	E_T/E_{20}	f_T/f_{20}	E_T/E_{20}	f_T/f_{20}
20	1.000	1.000	1.000	1.000	1.000	1.000	1.000	1.000
100	1.007	0.912	1.011	1.005	1.064	0.964	1.053	0.928
200	0.968	0.888	0.985	1.043	1.018	1.054	0.991	1.028
300	0.845	0.805	0.877	1.020	0.994	0.977	0.886	0.968
400	0.818	0.742	0.834	0.882	0.953	0.902	0.865	0.841
500	0.689	0.635	0.784	0.753	0.68	0.665	0.583	0.586
600	0.474	0.400	0.398	0.429	0.456	0.334	0.409	0.278

Table 3: The temperature factor for the coefficient of cold-formed effect for elastic modulus

T(°C)	$\beta_{1,E,T}=\frac{E_{1,T}/E_{1,20}}{E_{0,T}/E_{0,20}}$ (Q1)	$\beta_{1,E,T}=\frac{E_{2,T}/E_{2,20}}{E_{0,T}/E_{0,20}}$ (Q2)	$\beta_{1,E,T}=\frac{E_{3,T}/E_{3,20}}{E_{0,T}/E_{0,20}}$ (Q3)
20	1.000	1.000	1.000
100	1.004	1.057	1.046
200	1.018	1.052	1.024
300	1.038	1.176	1.048
400	1.020	1.165	1.057
500	1.138	0.987	0.846
600	0.840	0.962	0.863

Table 4: The temperature factor for the coefficient of cold-formed effect for yield strength

T(°C)	$\beta_{1,f,T}=\frac{f_{1,T}/f_{1,20}}{f_{0,T}/f_{0,20}}$ (Q1)	$\beta_{1,f,T}=\frac{f_{2,T}/f_{2,20}}{f_{0,T}/f_{0,20}}$ (Q2)	$\beta_{1,f,T}=\frac{f_{3,T}/f_{3,20}}{f_{0,T}/f_{0,20}}$ (Q3)
20	1.000	1.000	1.000
100	1.102	1.057	1.018
200	1.174	1.187	1.158
300	1.267	1.214	1.202
400	1.189	1.216	1.133
500	1.186	1.047	0.923
600	1.072	0.835	0.695

Table 5: The parameters for $\beta_{f,T}$ from linear fitting ($400℃ \leq T \leq 600℃$)

η_f	A_0	A_1
1.0336 (Q1)	1.3456	-4.1526E-4
1.3428 (Q2)	1.8362	-1.6400E-3
1.6483 (Q3)	2.1590	-2.4500E-3

Table 6: The parameters for $A_i(i=0,1)$ from linear fitting

η_f	A_0	A_1
1.3428 (Q2)	1.8362	-1.6400E-3
1.6483 (Q3)	2.1590	-2.4500E-3

Table 7: Comparison on the elastic modulus between predicted and tested results

T(°C)	Q1 (GPa)			Q2 (GPa)			Q3 (GPa)		
	Test	Prediction	Ratio	Test	Prediction	Ratio	Test	Prediction	Ratio
20	201	201	1.00	196	196	1.00	199	199	1.00
100	203	202	1.00	209	197	0.94	210	201	0.96
200	198	194	0.98	200	190	0.95	197	193	0.98
300	176	185	1.05	195	181	0.93	176	183	1.04
400	167	176	1.05	187	172	0.92	172	175	1.02
500	157	137	0.87	133	134	1.01	116	136	1.17
600	80	84	1.05	89	82	0.92	81	84	1.04
Mean value	-	-	1.00	-	-	0.95	-	-	1.03
Coefficient of variation	-	-	0.06	-	-	0.04	-	-	0.07

Table 8: Comparison on the yield strength between predicted and tested results

T(°C)	Q1 (MPa)			Q2 (MPa)			Q3 (MPa)		
	Test	Prediction	Ratio	Test	Prediction	Ratio	Test	Prediction	Ratio
20	353	353	1.00	459	459	1.00	564	564	1.00
100	355	322	0.91	443	419	0.95	523	514	0.98
200	369	360	0.98	484	467	0.96	579	574	0.99
300	360	339	0.94	449	440	0.98	546	540	0.99
400	312	309	0.99	414	402	0.97	474	493	1.04
500	266	254	0.95	305	300	0.98	330	331	1.01
600	152	153	1.01	153	161	1.05	157	152	0.97

Mean value	-	-	0.97	-	-	0.98	-	-	1.00
Coefficient of variation	-	-	0.04	-	-	0.03	-	-	0.02

Table 9: Dimensions of selected typical cold-formed thick-wall steel tube

Section label	Width (mm)	Height (mm)	Thickness (mm)	Length (mm)
S140×80×5	140	80	5	3000

Table 10: Mechanical properties of cold-formed thick-walled steels at ambient temperature

Specimen types	Base metal	Flat part	Corner part	Weld seam
Elastic modulus E (GPa)	203.1	206.0	211.1	209.3
The coefficient of cold-formed effect for elastic modulus $\eta_E = E/E(\text{Base metal})$	1.00	1.01	1.04	1.03
Yield strength f (MPa)	344.2	423.3	583.8	556.5
The coefficient of cold-formed effect for yield strength $\eta_f = f/f(\text{Base metal})$	1.00	1.23	1.69	1.62
Ultimate strength f_u (MPa)	498.0	516.1	611.6	680.3
The coefficient of cold-formed effect for ultimate strength $\eta_{f_u} = f_u/f_u(\text{Base metal})$	1.00	1.04	1.23	1.36

Table 11: Retention factors for the elastic modulus and yield strength

T(°C)	Base metal		Flat part		Corner part		Weld seam	
	E_T/E_{20}	f_T/f_{20}	E_T/E_{20}	f_T/f_{20}	E_T/E_{20}	f_T/f_{20}	E_T/E_{20}	f_T/f_{20}
20	1.000	1.000	1.000	1.000	1.000	1.000	1.000	1.000
100	1.007	0.912	1.011	1.005	1.064	0.964	1.053	0.928
200	0.968	0.888	0.985	1.043	1.018	1.054	0.991	1.028
300	0.845	0.805	0.877	1.020	0.994	0.977	0.886	0.968
400	0.818	0.742	0.834	0.882	0.953	0.902	0.865	0.841
500	0.689	0.635	0.784	0.753	0.68	0.665	0.583	0.586
600	0.474	0.400	0.398	0.429	0.456	0.334	0.409	0.278

Table 12: Validation of the elastic modulus prediction

T(°C)	Base metal (GPa)	Flat part (GPa)			Corner part (GPa)			Weld seam (GPa)		
	Test	Test	Prediction	Ratio	Test	Prediction	Ratio	Test	Prediction	Ratio
20	203	201	201	1.00	196	196	1.00	199	199	1.00
300	163	176	185	1.05	195	181	0.93	176	183	1.04
400	169	167	176	1.05	187	172	0.92	172	175	1.02
500	150	157	137	0.87	133	134	1.01	116	136	1.17
600	97	80	84	1.05	89	82	0.92	81	84	1.04
Mean value	-	-	-	1.00	-	-	0.95	-	-	1.03
Coefficient of variation	-	-	-	0.06	-	-	0.04	-	-	0.07

Table 13: Validation of the yield strength prediction

T(°C)	Base metal (GPa)	Flat part (MPa)			Corner part (MPa)			Weld seam (MPa)		
	Test	Test	Prediction	Ratio	Test	Prediction	Ratio	Test	Prediction	Ratio
20	344	423	423	1.00	584	584	1.00	556	556	1.00
300	296	419	446	1.06	559	615	1.10	555	586	1.05
400	277	380	402	1.06	492	554	1.12	495	529	1.07
500	244	296	320	1.08	349	377	1.08	327	370	1.13
600	151	171	177	1.04	188	165	0.88	167	170	1.02
Mean value	-	-	-	1.05	-	-	1.04	-	-	1.05
Coefficient of variation	-	-	-	0.03	-	-	0.09	-	-	0.05